

Space-time evolution and HBT analysis of relativistic heavy ion collisions in a chiral $SU(3)$ $SU(3)$ model.

D. Zschiesche, S. Schramm, H. Stoecker and W. Greiner

Institut für Theoretische Physik, Postfach 11 19 32, D-60054 Frankfurt am Main, Germany

(November 3, 2018)

Abstract

The space-time dynamics and pion-HBT radii in central heavy ion-collisions at CERN-SPS and BNL-RHIC are investigated within a hydrodynamic simulation. The dependence of the dynamics and the HBT-parameters on the EoS is studied with different parametrizations of a chiral $SU(3)$ model. The selfconsistent collective expansion includes the effects of effective hadron masses, generated by the nonstrange and strange scalar condensates. Different chiral EoS show different types of phase transitions and even a crossover. The influence of the order of the phase transition and of the difference in the latent heat on the space-time dynamics and pion-HBT radii is studied. A small latent heat, i.e. a weak first-order chiral phase transition, or even a smooth crossover leads to distinctly different HBT predictions than a strong first order phase transition. A quantitative description of the data, both at SPS energies as well as at RHIC energies, appears difficult to achieve within the ideal hydrodynamical approach using the $SU(3)$ chiral EoS. A strong first-order quasi-adiabatic chiral phase transition seems to be disfavored by the pion-HBT data from CERN-SPS and BNL-RHIC.

Typeset using REVTeX

I. INTRODUCTION

General theoretical arguments [1] and lattice QCD simulations [2] predict the occurrence of a transition of strongly interacting matter to a state where chiral symmetry is (approximately) restored. Since Bose-Einstein correlations in multiparticle production processes [3] provide valuable information on the space-time dynamics of fundamental interactions [4], correlations of identical pions produced in high energy collisions of heavy ions may provide information on the characteristics of that phase transition (for a review on QGP signatures, see [5]). For recent reviews on this topic we refer to [6,7].

In particular, a first order phase transition leads to a prolonged hadronization time as compared to a cross-over or a hadron gas with no symmetry restoration, and has been related to unusually large Hanbury-Brown-Twiss (HBT) radii [8,10]. The coexistence of hadrons and QGP reduces the "explosivity" of the high-density matter before hadronization, prolonging the emission duration of pions [8,10]. This phenomenon should then depend on the hadronization (critical) temperature T_c and the latent heat of the transition. Typically, calculations assuming a first-order phase transition are carried out with an equation of state (EoS) derived from matching the bag model with an ideal hadron gas model, for which the latent heat of the transition is large [9,10]. Consequently, the predicted HBT radii were large.

Here, we consider also the case of a more weak first-order transition with small latent heat and study the influence on the space-time characteristics of the expansion and on the HBT radii. Furthermore, we perform explicit calculations for smooth crossover transition at high temperatures, and discuss the resulting pion HBT radii. Such a scenario was considered in [10], however without explicit reference to chiral symmetry restoration and dynamical hadron masses.

To investigate the space-time dynamics and the influences of different types of phase transitions a hydrodynamic simulation with an EoS obtained from a chiral $SU(3)_L \times SU(3)_R$ model is employed. The equations of fluid dynamics describe the collective evolution of the

system, while the chiral $SU(3) \times SU(3)$ model yields the underlying equation of state. Thus, as the hot and dense central region expands both in the longitudinal and transverse directions, the hadrons approach their vacuum masses. The initial excitation energy is converted into both, collective flow and massive hadrons. This purely hadronic model describes successfully nuclear matter ground state properties, finite nuclei and hadron masses in the vacuum [17,18]. Furthermore, it exhibits different kinds of high temperature transitions, depending on the set of parameters. Using the various equations of state in a hydrodynamical simulation should discriminate between the different phase transition scenarios. Since the model only contains hadronic degrees of freedom, we only test the influence of the chiral phase transition but not of the deconfinement phase transition. In any case, the main effect as far as collective expansion is concerned, is due to the difference in the latent heat for the transition, irrespective of its microscopic origin.

This article is organized as follows. In section II we present our model. In particular, in IIA we discuss ideal relativistic hydrodynamics, and in IIB we refer to our equations of state. Section III shows our main results for the space-time evolution and the pion HBT radii. We summarize and conclude in section IV. Throughout the manuscript, we employ natural units $c = \hbar = k_B = 1$.

II. MODEL DESCRIPTION

A. Scaling Hydrodynamics

Ideal Hydrodynamics is defined by (local) energy-momentum and net charge conservation [11],

$$\partial_\mu T^{\mu\nu} = 0 \quad ; \quad \partial_\mu N_i^\mu = 0 \quad ; \quad (1)$$

$T^{\mu\nu}$ denotes the energy-momentum tensor, and N_i^μ the four-current of the i th conserved charge. We will explicitly consider only one such conserved charge, the net baryon number. We implicitly assume that the local densities of all other charges which are conserved on

strong-interaction time scales, e.g. strangeness, charm, and electric charge, vanish. The corresponding four-currents are therefore identically zero, cf. eq. (2), and the conservation equations are trivial.

For ideal fluids, the energy-momentum tensor and the net baryon current assume the simple form [11]

$$T = (E + p)u^\mu u^\nu - pg^{\mu\nu} ; N_B = N_B u^\mu ; \quad (2)$$

where E, p, N_B are energy density, pressure, and net baryon density in the local rest frame of the fluid, which is defined by $N_B = (N_B; 0)$. $g = \text{diag}(+; -; -; -)$ is the metric tensor, and $u = (1; \mathbf{v})$ the four-velocity of the fluid (\mathbf{v} is the three-velocity and $\gamma = (1 - \mathbf{v}^2)^{-1/2}$ the Lorentz factor). The system of partial differential equations (1) is closed by choosing an equation of state (EoS) in the form $p = p(E; N_B)$, cf. below.

For simplicity, we assume cylindrically symmetric transverse expansion with a longitudinal scaling flow profile, $v_z = z/t$ [12]. This should be a reasonable first approximation for central collisions at high energy (such as at CERN-SPS and BNL-RHIC energies), and around midrapidity. A quantitative comparison to experimental data, which we postpone to a future publication, should however analyze the effects due to coupling of longitudinal and transverse flows around midrapidity. At least up to CERN-SPS energies, $\sqrt{s} = 20 \text{ A GeV}$, such a coupling was shown to exist [13].

For the scaling expansion, at $z = 0$ equations (1) reduce to

$$\begin{aligned} \partial_t E + \partial_T [(E + p) v_T] &= \frac{v_T}{r_T} + \frac{1}{t} (E + p) ; \\ \partial_t M + \partial_T (M v_T + p) &= \frac{v_T}{r_T} + \frac{1}{t} M ; \\ \partial_t R + \partial_T (R v_T) &= \frac{v_T}{r_T} + \frac{1}{t} R ; \end{aligned} \quad (3)$$

where we defined $E = T^{00}$, $M = T^{0T}$, and $R = N_B^0$. In the above expressions, the index T refers to the transverse component of the corresponding quantity.

The set of equations (3) describes the evolution in the $z = 0$ plane. Due to the assumption of longitudinal scaling, the solution at any other $z \neq 0$ can be simply obtained by a Lorentz

boost. The above equations also imply [14]

$$\frac{\partial p}{\partial \tau} = 0 ; \tag{4}$$

where $\tau = A \operatorname{tanh} v_z$ and $p = \frac{p}{t^2 - z^2}$. This means that on proper-time hyperbolae pressure gradients in rapidity direction vanish, and there is no particle flow between adjacent infinitesimal rapidity slices. However, only for net baryon free matter, $\mu_B = 0$, does this automatically also mean that the temperature T is independent of the longitudinal rapidity y . In the case $\mu_B \neq 0$ equation (4) only demands

$$s \frac{\partial T}{\partial \tau} + \mu_B \frac{\partial \mu_B}{\partial \tau} = 0 ; \tag{5}$$

and s and μ_B denote entropy density and baryo-chemical potential, respectively. If other charges like strangeness or electric charge are locally nonvanishing, additional terms appear. Equation (5) does not imply that the rapidity distribution of produced particles is flat (i.e. independent of rapidity) or that the rapidity distributions of various species of hadrons, e.g. pions, kaons, and nucleons, are similar. Any rapidity-dependent T and μ_B that satisfy eq. (5) are in agreement with energy-momentum and net baryon number conservation, as well as with longitudinal scaling $\rho \propto v_z = z = t$. In this paper, however, we do not explore the rapidity dependence of the particle spectra, and thus, as discussed below, are not required to specify T and μ_B as functions of y .

The hydrodynamic equations of motion are solved on a discretized space-time grid ($r_T = R_T = 100 = 0.06 \text{ fm}$, $\Delta \tau = 0.99 r_T$) by employing the RHLL algorithm as described and tested in [10,15]. We have checked that the algorithm accurately conserves total energy and baryon number, and that profiles of rarefaction and shock waves are reproduced accurately for various initial conditions [14,16].

As already mentioned above, eqs. (2), we assume a perfect, i.e. non-dissipative, relativistic fluid. In principle, it is possible to calculate the transport coefficients from the lagrangian of our model [17,18]. (For example, various transport coefficients have been computed in the symmetry broken phase based on the assumption of an ideal gas of hadrons [19].) Also, dynamical simulations indicate that dissipation strongly affects the pion correlation functions

at small relative momentum, and thus the deduced HBT radii [20]. Quantitative comparisons to experimental data should therefore account for dissipative effects. On the other hand, the purpose of this paper is to explore the effects from varying the latent heat and the order of the phase transition. In that vein, we can leave aside the great technical and principal difficulties related to a treatment of dissipation in dynamical simulations [42], and give an impression of the largest possible effects of varying the phase transition parameters that can be expected. This will also allow for a comparison to previous results for the pion HBT correlation functions, which employed ideal fluid dynamics with an EoS derived from the bag model [9,10].

B. Equations of state from a chiral SU(3) SU(3) model

To close the system of coupled equations of hydrodynamics, an equation of state (EoS) has to be specified. Lattice QCD predicts a phase transition from ordinary nuclear matter to a so-called quark-gluon plasma (QGP) at a critical temperature of $T_c = 140 - 160$ MeV [2,21] (for $\mu_B = 0$). We obtain the equation of state from a chiral SU(3) SU(3) σ model that was discussed in detail in [17,18]. We will briefly introduce the model here: consider a relativistic field theoretical model of baryons and mesons based on a nonlinear realization of chiral symmetry and broken scale invariance. The general form of the Lagrangean looks as follows:

$$L = L_{\text{kin}} + \sum_{M=X,Y,V,A,u} L_{BM} + L_{\text{vec}} + L_{VP} - V_0 - V_{SB} \quad (6)$$

L_{kin} is the kinetic energy term, L_{BM} includes the interaction terms of the different baryons with the various spin-0 and spin-1 mesons. The baryon masses are generated by both, the nonstrange ($\langle qq \rangle$) and the strange ($\langle ss \rangle$) scalar condensate. X, Y, V, A, u stand for scalar octet, scalar singlet, vector, axial vector and pseudoscalar mesons respectively. L_{VP} contains the interaction terms of vector mesons with pseudoscalar mesons. L_{vec} generates the masses of the spin-1 mesons through interactions with spin-0 mesons, and V_0 gives the

meson-meson interaction terms which induce the spontaneous breaking of chiral symmetry. It also includes a scale-invariance breaking logarithmic potential. Finally, V_{SB} introduces an explicit symmetry breaking of the $U(1)_A$, the $SU(3)_V$, and the chiral symmetry. All these terms have been discussed in detail in [17,18].

The hadronic matter properties at finite density and temperature are studied in the mean-field approximation, i.e. the meson field operators are replaced by their expectation values and the fermions are treated as quantum mechanical one-particle operators [22]. After performing these approximations, the Lagrangean (6) becomes

$$\begin{aligned}
 L_{BM} &= \sum_i \bar{\psi}_i [g_i \sigma + g_i \rho + m_i] \psi_i \\
 L_{vec} &= \frac{1}{2} m_\pi^2 \left(\frac{\sigma}{f_\pi} \right)^2 + \frac{1}{2} m_\rho^2 \left(\frac{\rho}{f_\rho} \right)^2 + g_4^4 (\sigma^4 + 2 \rho^4) \\
 V_0 &= \frac{1}{2} k_0 \sigma^2 (\sigma^2 + \rho^2) + k_1 (\sigma^2 + \rho^2)^2 + k_2 \left(\frac{\sigma^4}{2} + \rho^4 \right) + k_3 \sigma^2 \\
 &\quad + k_4 \rho^4 + \frac{1}{4} \sigma^4 \ln \frac{\sigma^4}{4} - \frac{1}{3} \rho^4 \ln \frac{\rho^2}{2} \\
 V_{SB} &= - \frac{m^2 f}{2} + \left(\frac{p}{2m_K^2} f_K - \frac{1}{2} m^2 f \right) \sigma ;
 \end{aligned}$$

with m_i the effective mass of the baryon i ($i = N, \Sigma, \Lambda, \Xi, \Omega$). σ and ρ correspond to the scalar condensates, σ and ρ represent the iso-singlet non-strange and the strange vector field, respectively, and ϕ is the dilaton field, which can be viewed as representing the effects of the gluon condensate. In this work we will use the frozen glueball approximation, i.e. adopt the dilaton field as constant. In the current form of the model this makes sense, since the glueball field does not change strongly with temperature and density. In a forthcoming work we will investigate the consequences of a stronger coupling of the glueball field to the scalar fields.

The thermodynamical potential of the grand canonical ensemble per volume V at a given chemical potential μ and temperature T can be written as:

$$\bar{\omega} = \frac{1}{V} (L_{vec} + V_0 + V_{SB} - V_{vac})$$

$$\frac{1}{T} \sum_i \frac{g_i}{(2\pi)^3} \int d^3k \ln [1 + e^{-\frac{1}{T} E_i(k)}] + \frac{1}{T} \sum_j \frac{g_j}{(2\pi)^3} \int d^3k \ln [1 - e^{-\frac{1}{T} E_j(k)}]$$

The vacuum energy V_{vac} (the potential at $\phi = 0$) has been subtracted in order to get a vanishing total vacuum energy. g_i denote the fermionic and g_j the bosonic spin-isospin degeneracy factors. The single particle energies are $E_i(k) = \sqrt{k_i^2 + m_i^2}$, with $m_i = m_i(\phi)$ (see [17,18]). The effective baryonic chemical potentials read $\mu_i = \mu_i - g_i!$ g_i with $\mu_i = (n_q^i - n_{\bar{q}}^i)_{q} + (n_s^i - n_{\bar{s}}^i)_{s}$ and the mesonic chemical potentials read $\mu_j = (n_q^j - n_{\bar{q}}^j)_{q} + (n_s^j - n_{\bar{s}}^j)_{s}$. $n_q^i, n_{\bar{q}}^i, n_s^i$ and $n_{\bar{s}}^i$ denote the number of constituent q, \bar{q}, s and \bar{s} quarks in particle species i , respectively.

The mesonic fields are determined by extremizing $\bar{v}(\phi; T)$: The density of particle i can be calculated by differentiating \bar{v} with respect to the corresponding chemical potential μ_i . This yields:

$$n_i = \frac{g_i}{(2\pi)^3} \int d^3k \frac{1}{\exp[(E_i - \mu_i)/T] + 1}$$

The net density of particle species i is the given by $n_i - \bar{n}_i$. The energy density and the pressure follow from the Gibbs(Duhem) relation, $\bar{v} = \bar{v} + TS + \sum_i \mu_i n_i$ and $p = -\bar{v}$. The model shows a phase transition or a crossover around $T_c = 150 \text{ MeV}$. Since there are only hadronic degrees of freedom in the model, this phase transition is of purely hadronic nature, i.e. the strong increase of the scalar density reduces the masses of the baryons, which in turn again increases the scalar density (compare e.g. to [23]).

The characteristics (e.g. the order, the latent heat) of the various phase transitions depend on the chosen parameters and on the considered degrees of freedom. We will use three different parameter sets, which differ in their treatment of the baryon resonances. This leads to different predictions concerning the behavior of hot hadronic matter. In parameter set C I the baryon decuplet is neglected, and the only degrees of freedom in the system are the members of the (anti)-baryon octet, the pseudoscalar meson nonet and the vector meson nonet. In parameter set C II and C III we include the (anti)-baryon decuplet. This

increases the number of degrees of freedom by 80. The parameter sets C II and C III differ in the treatment of the strange spin- $\frac{3}{2}$ resonances. In parameter set C II an additional explicit symmetry breaking is included which is neglected in parameter set C III. In figure 1 the resulting pressure and energy density are plotted as a function of temperature for vanishing chemical potential. The predicted behavior of the hot hadronic matter differs significantly for the different parameter sets. Parameter set C I exhibits a smooth crossover, a first order phase transition is found for parameter set C II. Two first order phase transitions are found for parameter set C III. This surprising behavior is due to the strange scalar condensate. In the SU(2) case only one phase transition occurs, driven by the scalar density. Now we have an additional scalar condensate: Since this strange condensate couples only weakly to the nonstrange baryons, its decrease is mainly driven by the scalar density of the hyperons, which significantly increases at a higher temperature than the scalar density of the nonstrange baryons. Therefore the strange condensate might also show a discontinuity, which occurs at a different temperature than the discontinuity in the nonstrange scalar condensate. This is just what happens for parameter set C III. Therefore here two phase transitions occur, corresponding to the separate jumps in the non-strange and strange condensates. The resulting velocities of sound are shown in figure 2.

FIGURES

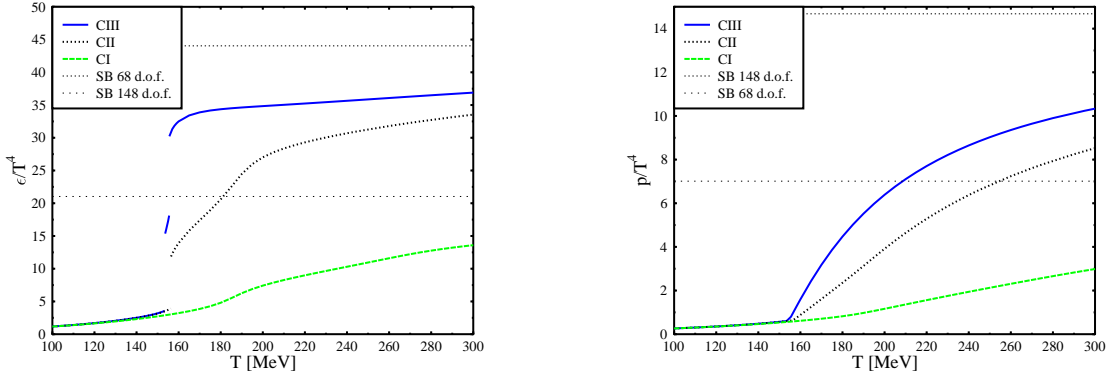


FIG .1. $\epsilon=T^4$ and $p=T^4$ for the three different parameter sets C I, C II, C III at $q = s = 0$. Depending on the chosen parameters we observe a different phase transition behavior. For C I no jump occurs in the energy as a function of the temperature, i.e. a smooth crossover takes place. In contrast C II leads to a jump in $\epsilon=T^4(T)$ at $T \approx 150$ MeV and a discontinuity in the rise of $p=T^4$ with T . Finally, C III even shows two discontinuities in $\epsilon=T^4(T)$. The horizontal lines correspond to the Stefan-Boltzmann limit with and without the (anti)-baryon decuplet.

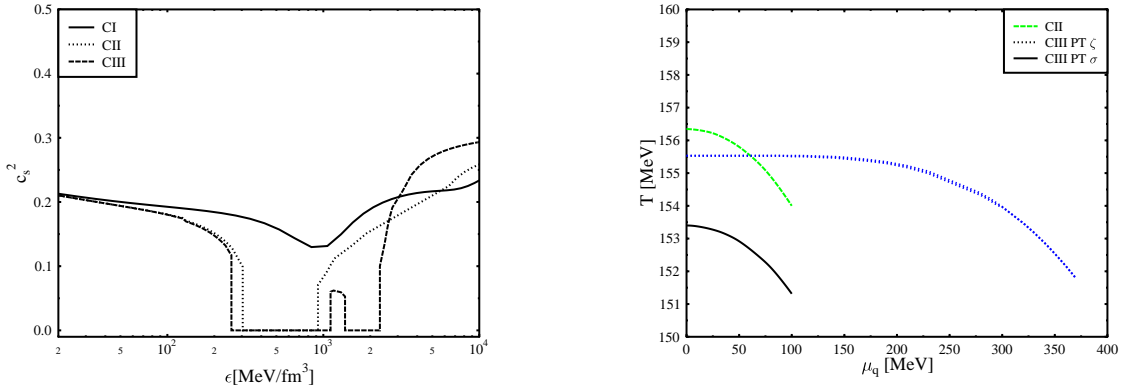


FIG. 2. Left: c_s^2 for three different equations of state at $\mu_q = \mu_s = 0$. The different high temperature behavior reflects in the energy-density dependence of the square of the velocity of sound. For the crossover case, c_s^2 decreases slightly, around $\epsilon = 1 \text{ GeV} = \text{fm}^3$, but always stays finite. For C II and C III, the occurrence of a phase transition leads to a vanishing c_s^2 . For C III this happens even twice, since two phase transitions occur. Right: Phase diagram for the parameter sets C II and C III for $f_s = 0$. The occurrence of a first order phase transition depends on the chemical potential. For small chemical potential, $\mu_q < 100 \text{ MeV}$, C III shows two phase transitions due to the jump in the ϵ and the ϵ field while C II exhibits one PT due to the jump in the ϵ field. At higher chemical potentials, ($100 \text{ MeV} < \mu_q < 370 \text{ MeV}$) C III shows a phase transition due to the jump in the ϵ field. The two chemical potentials ($\mu_q; \mu_s$) of the system lead to a slight change of the temperature in the phase transition region (mainly around $\mu_q \approx 200 \text{ MeV}$).

The crossover EoS shows a decrease of c_s^2 around $\epsilon = 1 \text{ GeV} = \text{fm}^3$. This is due to the strong reduction of the baryonic masses around the phase transition region. However, because the latent heat is zero in the crossover case, c_s^2 remains finite. In contrast c_s^2 vanishes in the phase transition regions for C II and C III. The latent heat for C II is $E_{\text{II}} = 600 \text{ MeV} = \text{fm}^3$, while it is $E_{\text{III}} = 850 \text{ MeV} = \text{fm}^3 + 920 \text{ MeV} = \text{fm}^3 = 1770 \text{ MeV} = \text{fm}^3$ for C III (Both values are for $\mu_q = \mu_s = 0$). Between the two distinct first-order transitions in model III, c_s^2 is non-zero again. However, this happens in a very narrow interval of energy density, and plays no significant role in our analysis but can be important for the re-occurrence of the directed flow and squeeze-out in full edged 3+1 dimensional 3-uid hydrodynamical calculations. As can be seen from Fig 2 r.h.s., the occurrence of a first order phase transition depends on the chemical potential. For small chemical potential, $\mu_q < 100 \text{ MeV}$, C III shows two phase transitions due to the jump in the ϵ and the ϵ field while C II exhibits one PT due to the jump in the ϵ field. At higher chemical potentials, ($100 \text{ MeV} < \mu_q < 370 \text{ MeV}$) C III shows a phase transition due to the jump in the ϵ field. Furthermore, since in the SU(3)-approach two chemical potentials ($\mu_q; \mu_s$) have to be considered, the condition $f_s = 0$ does not hold for each phase in the mixed-phase region, but only globally. This leads to a slight change of

the temperature in the mixed phase. For chemical potential $\mu_q > 370 \text{ MeV}$ there is no phase transition for $f_s = 0$. The energy densities and entropy densities in the phase transition regions are specified in table I.

TABLES

	ϵ_0	ϵ_0^+	s	s^+	T_c [MeV]
C II	2.1	6.3	2.3	6.2	156.3
C III	1.7	7.6	2.0	7.5	153.4
	9.4	15.7	9.3	15.2	155.5

TABLE I. Energy density and entropy per net baryon in the phase transition regions for the three sets of chiral parameters for vanishing chemical potentials $\mu_q = \mu_s = 0$. The () ; (+) signs stand for values below and above the phase transition, respectively. T_c denotes the phase transition temperature. $\epsilon_0 = 147 \text{ MeV}/\text{fm}^3$ denotes the energy density of nuclear matter in the ground state.

The effective potential for parameter set C II around the phase transition temperature T_c is depicted in figure 3.

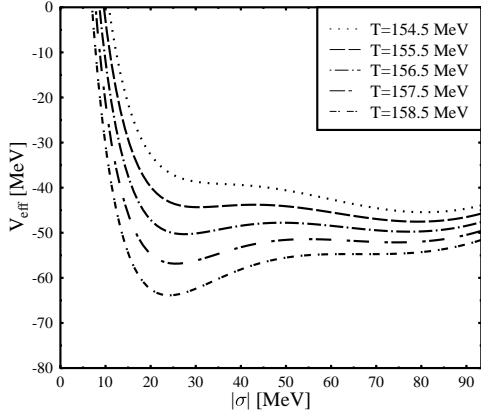


FIG. 3. Effective Potential V_{eff} as a function of the scalar condensate around T_c . For parameter set C II and $q = s = 0$.

We observe that the effective potential varies very rapidly around T_c . The spinodal points, i.e. the temperatures at which the inflection points for the two minima appear, are only 2–3% of T_c . This potential therefore varies substantially faster than that from the Gross-Neveu model or from the SU(2) linear sigma model investigated in [24]. However, the variation of the potential around T_c obtained from our model is in the same range as for the model used in [27], where the authors showed that such a fast variation of the effective potential around T_c might lead to explosive behavior via rapid spinodal decomposition (as opposed to an adiabatic phase transition). This questions the applicability of our approach of equilibrium hydrodynamics. However, as a first approximation, we study the effects dynamically, assuming that local equilibrium does hold, i.e. that the mean fields in fact assume the value of the global minimum of the potential, and that at the critical temperature two phases (corresponding to the two minima of the effective potential) coexist.

C . Initial C onditions

The initial conditions in scaling hydrodynamics are specified on a proper-time hyperbola $\tau = \tau_i$, as suggested by equation 4. On that space-like hypersurface one has to specify the entropy per net baryon and the net baryon rapidity density at midrapidity, dN_B/dy . A model with a MIT bag model equation of state [28] for the high temperature phase and an ideal hadron gas in the low temperature region can reproduce both [14], the measured transverse energy at midrapidity, and the p_T -spectra of a variety of hadrons at $\sqrt{s} = 17.4A$ GeV (CERN-SPS energy), assuming the standard thermalization (proper) time $\tau_i = 1$ fm/c, an entropy per net baryon of $s_B = 45$ and a net baryon rapidity density $dN_B/dy = 80$. This value for s_B is also in good agreement with the measured relative abundancies of hadrons [29]. The initial net baryon density follows as $n_B = 4.5 \rho_0$. The corresponding values of $\mu_i, T; \mu_q$ and μ_s (q- and s-quark chemical potential respectively) for the various chiral EoS are listed in table II. The initial net baryon density is independent of the underlying EoS because the continuity equation for the net baryon current in (1,3) does not involve the pressure p .

Due to the higher density at midrapidity, thermalization may be faster at BNL-RHIC energies { following [10] we assume $\tau_i = 0.6$ fm/c. Various microscopic models, e.g. PCM [30], RQMD [31], FRITIOF 7.02 [32], and HLJING/B [33], predict a net baryon rapidity density of $dN_B/dy = 20 - 35$ and specific entropy of $s_B = 150 - 250$ in central Au+Au at $\sqrt{s} = 130A$ GeV at midrapidity. We will employ $s_B = 200$ and $dN_B/dy = 25$. The resulting baryon density at midrapidity is $n_B = 2.3 \rho_0$. Hadron multiplicity ratios at midrapidity can be described with these initial conditions [43]. Furthermore, it was recently shown that HBT correlations of pions at small relative momenta do not depend sensitively on these initial conditions [20]. The energy density and baryon density are initially distributed in the transverse plane according to a so-called "wounded nucleon" distribution with transverse radius $R_T = 6$ fm. For further details, we refer to refs. [14,20].

		μ_0	p_0	T [M eV]	q [M eV]	s [M eV]
SPS	C I	49.2	10.5	256.0	236.2	133.0
	C II	40.2	6.6	197.0	241.3	58.6
	C III	37.3	5.9	180.6	246.6	36.4
RHIC	C I	127.9	29.3	313.3	138.4	95.8
	C II	100.4	21.4	242.0	151.6	60.9
	C III	93.7	22.0	230.0	154.6	53.0

TABLE II. Initial values for the three sets of chiral parameters, corresponding to $s_B = 45$ and $dN_B/dy = 80$ for CERN-SPS energy and $s_B = 200$ and $dN_B/dy = 25$ for BNL-RHIC energy. $\mu_0 = 147$ M eV / fm³ is the energy density of nuclear matter in the ground state.

As seen from table II, the initial energy density more than doubles when going from CERN-SPS energy to BNL-RHIC energy. The initial temperature increases by about 50 MeV, while the initial chemical potential for u, d quarks decreases by about 100 MeV, in all cases. Note that for a bag model EoS the chemical potential for s -quarks vanishes because of strangeness neutrality in the QGP phase, see e.g. [14]. Evaporation of kaons, however, can yield finite n_s even before the phase coexistence region is reached, i.e. when strangeness distillation sets in [25], driving the system away from the $f_s = 0$ plane. In a hadronic model, the hyperons contain non-strange quarks and adopt a finite chemical potential if $\mu_q \neq 0$. Therefore, the hyperon vector density is positive at finite temperature. This surplus of strange quarks contained in the hyperons is balanced by the anti-strange quarks in strange mesons. This leads to a finite strangeness chemical potential μ_s , which is adjusted to yield $n_s = -n_{\bar{s}}$. Here $n_s; n_{\bar{s}}$ denote the total number of strange and anti-strange quarks in the system, respectively. As already mentioned in [25] in the mixed phase netto strangeness f_s is only globally equal to zero, i.e. the two phases in equilibrium may adopt finite values for f_s . Furthermore for the case of a first order phase transition the evaporation of pions and kaons and strangeness distillation [25] should be studied, since these influence the unlike particle correlations (e.g. $K^+ = -K^-$, see [26]).

III. RESULTS

A. Hypersurfaces

Figure 4,5 show the calculated hypersurfaces at fixed temperature, $T = T_f$, in the transverse plane at $\mu = 0$ for the three chiral EoS. $T_f = 80$ MeV, 100 MeV and 130 MeV respectively for CERN-SPS energies. Figures 6,7 show the analogous calculations for BNL-RHIC energies.

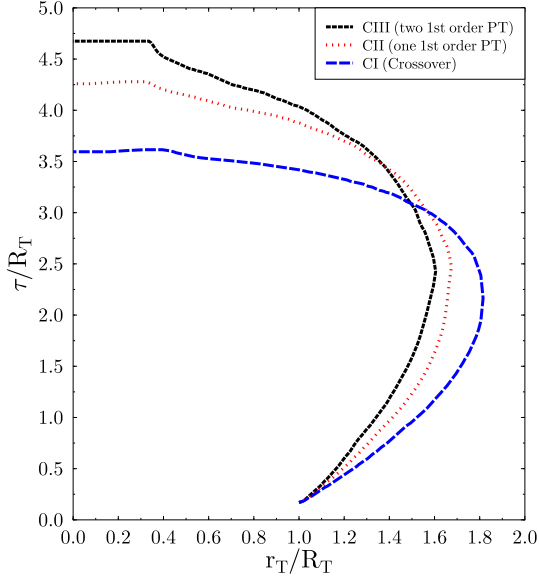


FIG . 4. Hypersurfaces $T = T_f$ for the three chiral EoS, $T_f = 80\text{M eV}$. This figure corresponds to initial conditions as appropriate for central Pb+Pb collisions at CERN-SPS energy ($\sqrt{s} = 17.4\text{AG eV}$).

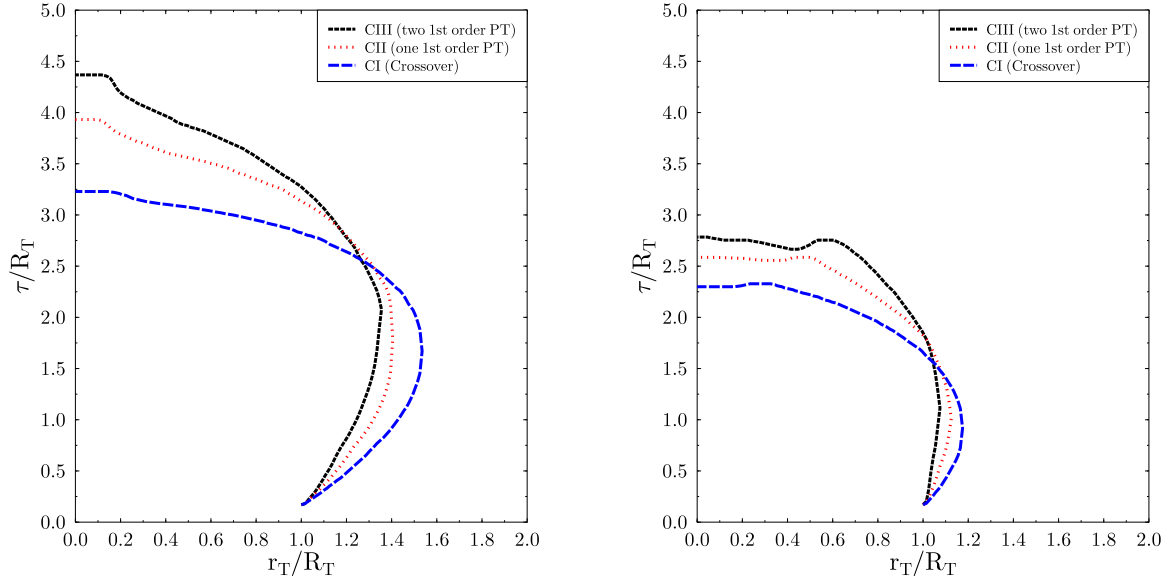


FIG . 5. Hypersurfaces $T = T_f$ for the three chiral EoS, $T_f = 100\text{M eV}$ (left) and $T_f = 130\text{M eV}$ (right). This figure corresponds to initial conditions as appropriate for central Pb+Pb collisions at CERN-SPS energy ($\sqrt{s} = 17.4\text{AG eV}$).

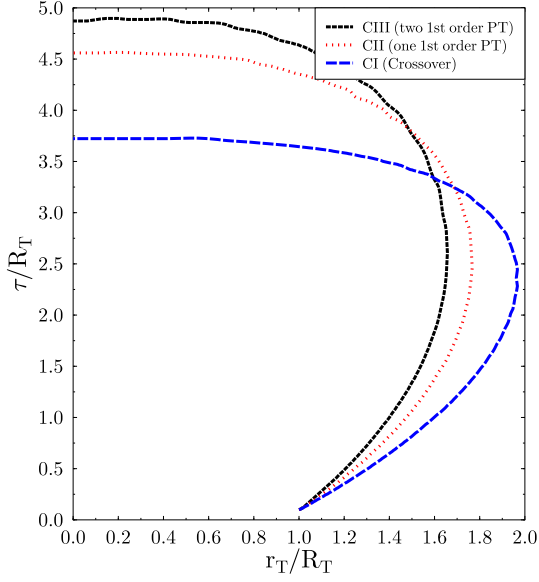


FIG . 6. Hypersurfaces $T = T_f$ for the three chiral EoS, $T_f = 80\text{M eV}$. This figure corresponds to initial conditions as appropriate for central Au+Au collisions at BNL-RHIC energy ($\sqrt{s} = 130\text{AG eV}$).

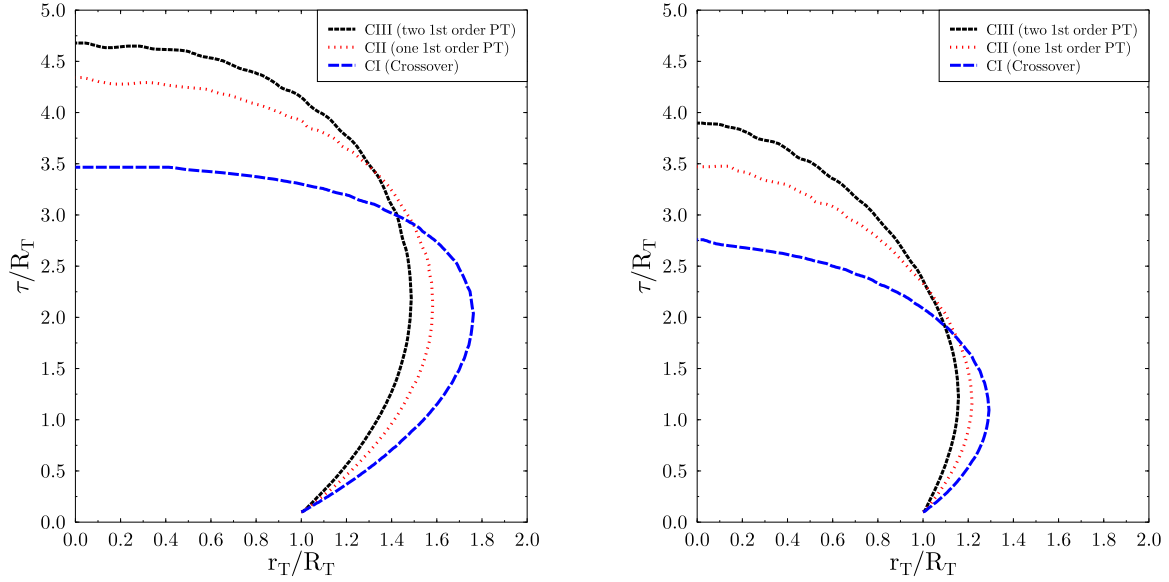


FIG . 7. Hypersurfaces $T = T_f$ for the three chiral EoS, $T_f = 100\text{M eV}$ (left) and $T_f = 130\text{M eV}$ (right). This figure corresponds to initial conditions as appropriate for central Au+Au collisions at BNL-RHIC energy ($\sqrt{s} = 130\text{AG eV}$).

Comparing the freeze-out curves for the different equations of state one finds that the different phase-transition behavior of the three parameter sets is reflected in the space-time evolution of the system. In case I (crossover) the time until freeze-out is shorter than in case III (two first order phase transitions). This is not surprising, since the occurrence of a mixed phase prolongs the expansion time and the jump in the entropy density can be directly related to the time the system stays within the mixed phase (τ_{+}). E.g. for 1+1 dimensional scaling one obtains $\tau_{+} = \tau_{-} + \tau_{+}$; where s_{+} , s_{-} denote the entropy densities of the restored symmetry and broken symmetry phases, respectively, on the phase boundary. The fastest expansion is obtained for a crossover with no latent heat and, accordingly, no discontinuity in the entropy density. In that case, $s_{+} = s_{-}$ and thus $\tau_{+} = \tau_{-}$. The expansion is not delayed at the phase boundary. On the other hand, the expansion is delayed most strongly for the largest discontinuity in the entropy density, such that the central region spends a time fraction of $s_{+} = s_{-}$ at the phase boundary, before cooling further.

The different space-time evolutions for the three EoS is most obvious for $T_f = 80$ MeV and $T_f = 100$ MeV but can also be seen for $T_f = 130$ MeV. Comparing the time evolution at SPS and RHIC, we see that due to the higher initial entropy at RHIC the evolution from the initial space-like surface $\tau = 0$ to the surface $T = T_f$ takes longer, for all three temperatures and all three different EoS. The differences in the time until freeze-out between RHIC and SPS energies are the longer, the larger the chosen freeze-out temperature. The size of the system at T_f is also increased at RHIC energies as compared to SPS. Comparing these results to [14], who employed a bag model EoS with $T_c = 160$ MeV and latent heat $E_{\text{Bag}} = 1.3 \text{ GeV} = \text{fm}^3$, we find that for SPS energies the time until freeze-out is reduced for all three chiral EoS. For RHIC energies the situation changes. Here only for the crossover EoS T_f is reached faster than for the bag model EoS [14], while for the C II (phase transition with moderate latent heat) EoS we find a similar spacetime evolution as in [14]; and for case III with two first order phase transitions and a higher latent heat the expansion takes longer compared to the same calculation in [14]. This is due to the MIT bag model value of

$c_s^2 = \frac{1}{3}$ above T_c , which is considerably larger than for the chiral models (see Fig. 2). This leads to a faster expansion for the bag EoS especially for RHIC, since there the system is initialized quite far above T_c and therefore spends a larger fraction of the expansion in this phase. This explains why the time until freeze-out in the bag model is comparable to the C II case, even though the latent heat is much larger for the Bag Model EoS than for C II.

B. Two particle correlations

To calculate the two particle correlation function we use the method developed in [4,8]. We measure the coincidence probability $P(p_1; p_2)$ of two identical particles with momenta $p_1; p_2$ relative to the probability of detecting uncorrelated particles. As is known from [37,8], the width of the correlation function in out-direction (R_{out}) is inversely proportional to the duration of the particle emission, i.e. to the lifetime of the source. Analogously, the inverse width of the correlation function in side-direction (R_{side}) is a measure for the (transverse) size of the source. Using a Gaussian fit one can relate the inverse widths of the correlation functions to radius parameters. It was pointed out in [10] that both for model calculation as well as for experimental data it is tedious, if not impossible, to relate R_{side} and R_{out} to the real source size and lifetime. However, the ratio $R_{side}=R_{out}$ can be used as a measure for the lifetime of the system.

The HBT radii shown below are obtained as follows. We assume that the pion correlation function is determined on a hypersurface of given temperature T_f , where the pion mean free path supposedly becomes too large to maintain local equilibrium. As already mentioned above, at present we refrain from a detailed study of transport coefficients of our model. Rather, our approach shall be more pragmatic, and we shall consider T_f as a free parameter. We shall show results for $T_f = 130$ MeV, $T_f = 100$ MeV as well as for $T_f = 80$ MeV, and compare the results to experimental data.

On the $T = T_f$ hypersurface, the two-particle correlation function is given by [9,10]

$$C_2(p_1; p_2) = 1 + \frac{1}{N} \int d^4x \int d^4y \langle K(x) K(y) \rangle \quad (7)$$

The normalization factor N is given by the product of the invariant single-particle inclusive distributions of the pions evaluated at momenta p_1 and p_2 , respectively. u denotes the four-velocity of the fluid on the $T = T_f$ surface, $K = (p_1 + p_2)/2$, $q = p_1 - p_2$ are the average four-momentum and the relative four-momentum of the pion pair, respectively. For midrapidity pions, $K_k = q_k = 0$. Thus, for the cylindrical geometry, the correlation function depends on three variables only; that is, the out and side components of q , and the transverse momentum of the pion pair, K_T . In (7), f denotes the local distribution function of pions in momentum space, at a temperature T_f . For simplicity, we shall assume a thermal distribution function and neglect the interaction energy of the pions, which amounts to only a 5% correction relative to the vacuum mass of the pion. From $C_2(q_{out}; q_{side}; K_T)$ we determine the HBT radii as $R_{out} = \sqrt{\frac{p}{\ln 2} q_{out}}$ and $R_{side} = \sqrt{\frac{p}{\ln 2} q_{side}}$, where q_{out} , q_{side} are defined by $C_2(q_{out}; q_{side} = 0) = C_2(q_{side}; q_{out} = 0) = 3/2$.

In Fig. 8,9 we show the resulting HBT radii R_{side} and R_{out} for central Pb+Pb collisions at SPS energy ($\sqrt{s} = 17.4$ GeV), and compare to recent preliminary data obtained by the NA49 collaboration [34]. Of course, in view of the approximations mentioned above such a comparison should be interpreted with care.

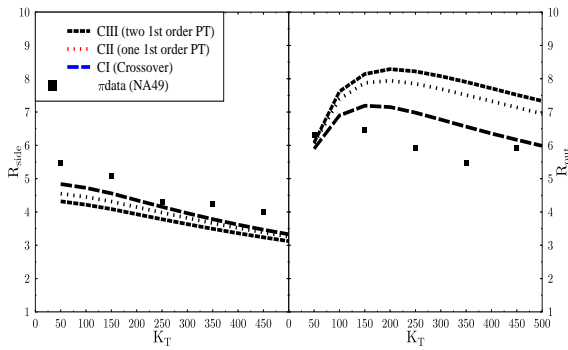


FIG. 8. R_{side} and R_{out} as a function of K_T at SPS. $T_f = 80$ MeV.

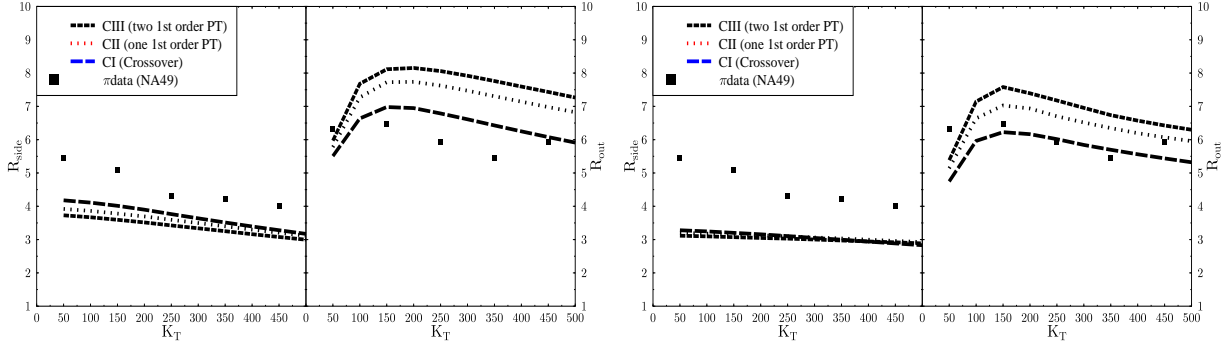


FIG . 9. R_{out} and R_{side} as a function of K_T at SPS. $T_f = 100M eV$ (left) and $T_f = 130M eV$ (right).

At $T_f = 130 M eV$, R_{out} is reproduced reasonably well. In particular, it appears that the EoS with the largest latent heat overestimates R_{out} . This is rather similar to the bag model EoS [10,20]. Note that R_{out} describes the size of the source folded with the mean emission duration [37,8{10,7,20}]. From Fig. 5, the average radius of the pion source decreases with increasing latent heat, but the emission duration increases. Integrating over the emission surface, Fig. 9 shows that for $K_T \approx 50 M eV$ the latter dominates in case of longitudinal scaling expansion, and R_{out} increases with the latent heat of the chiral transition. The best description of the data is found for vanishing or small latent heat, i.e. for a smooth transition or at least small latent heat.

At $T_f = 80 M eV$ and $T_f = 100 M eV$, see Fig. 9 and the l.h.s. of Fig. 8, the pion source has expanded further, as is also obvious from Fig. 4 and Fig. 5, and hence R_{out} is larger. At large K_T , the EoS with first-order phase transition predicts too large values for R_{out} for both values of T_f . At small transverse momenta, on the other hand, all three EoS describe the data better than for the high freeze out temperature. This observation is in agreement with the results of ref. [20], which shows that due to dissipative effects particles which suffer soft hadronic rescatterings freeze out at much later times than particles subject to harder interactions. We can not account for that effect within our ideal-uid model, but it can be mimicked by choosing a lower T_f at smaller K_T . In any case, our main focus is on effects

from the chiral phase transition. Our results suggest that a weakly first-order transition, or a smooth crossover, can give a better description of R_{out} than a phase transition with large latent heat (as in the bag model).

R_{side} measures the geometric size of the pion source in the transverse plane¹, and does not depend on the emission duration [37,8{10,7,20}]. First, we note that the effective source radius depends only very weakly on the latent heat for the transition, in particular for large T_f . This is in accord with the space-time evolution depicted in Fig. 5. At small K_T , R_{side} increases slightly with the latent heat. However, for all three EoS, R_{side} comes out too small. Only for $T_f = 80$ MeV a satisfactory description is obtained. This could be partly due to the neglect of resonance decays, which form a "halo" surrounding the direct pion source [9,7,36], and increase its effective size. On the other hand, the resonance decays would also tend to increase R_{out} . As discussed in [10], a reasonable measure for the emission duration of pions therefore is the ratio $R_{out}=R_{side}$, which is also less affected by resonance decays.

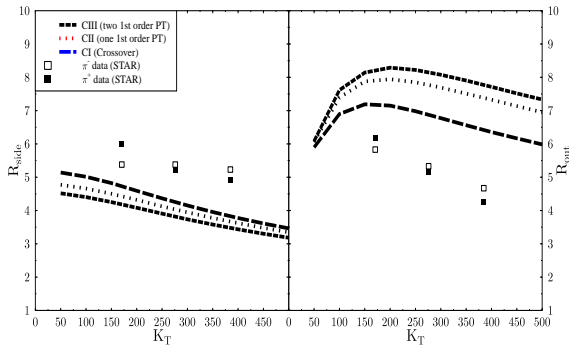


FIG. 10. R_{side} and R_{out} as a function of K_T at RHIC. $T_f = 80$ MeV.

¹More precisely, it corresponds to the scale of spatial homogeneity [35].

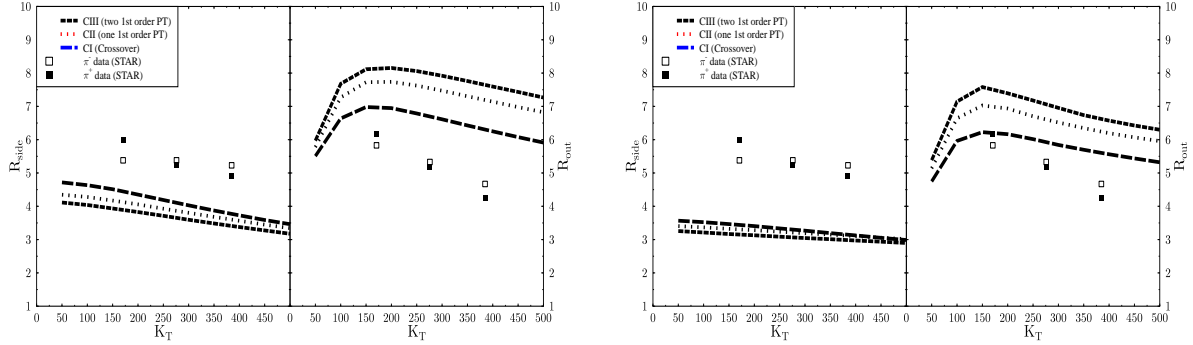


FIG .11. R_{side} and R_{out} as a function of K_T at RHIC. $T_f = 100$ MeV (left) and $T_f = 130$ MeV (right).

In Fig. 11 we show the results for initial conditions appropriate for BNL-RHIC energies. Both radii increase as compared to the lower SPS energy. That is because the initial entropy density is significantly larger. Thus the system takes longer to cool down to T_f , and the system has more time to expand in the transverse direction. For example, at $K_T = 500$ MeV, R_{out} increases by about 1 fm for the EoS with a strongly first-order phase transition. R_{side} increases even less. This is in contrast to an EoS with only pions in the hadronic phase [37,8,10], where the ratio of entropies of the two thermodynamic phases is very large at T_c . The very moderate increase of the radii from SPS to RHIC energy is in agreement with the preliminary results from STAR for Au+Au collisions at RHIC [38]. On the other hand, as already discussed above, the "geometric size" of the source, R_{side} , is too small. As at SPS energy, this could be due to decays of resonances. We shall therefore discuss next the behavior of the ratio R_{out}/R_{side} with K_T , which is less affected by decays [10], and which is a good measure for the lifetime of the pion source.

Figures 12,13 and 14, 15 show the experimentally measured ratio R_{out}/R_{side} as a function of K_T for the three different equations of state for SPS and RHIC energies.

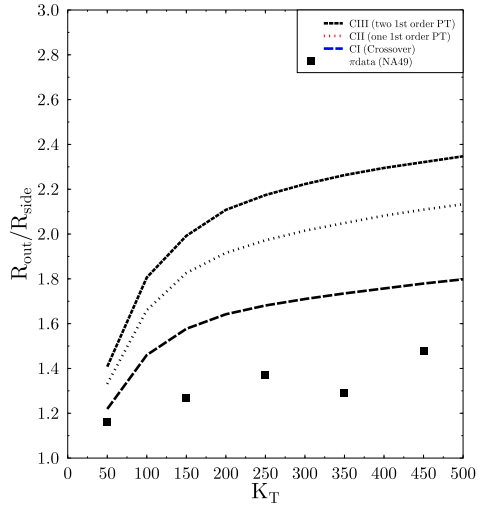


FIG .12. $R_{out}=R_{side}$ as a function of K_T at SPS for $T_f = 80M$ eV .

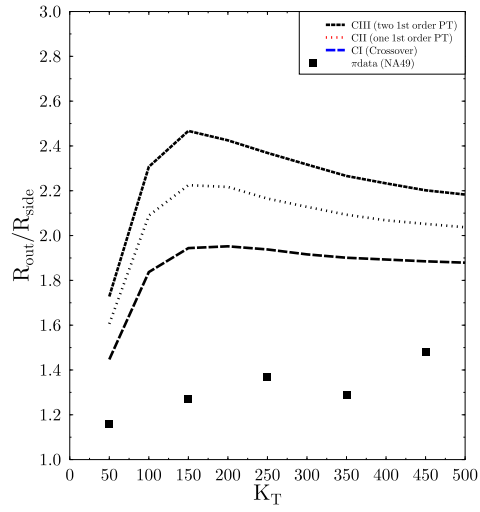
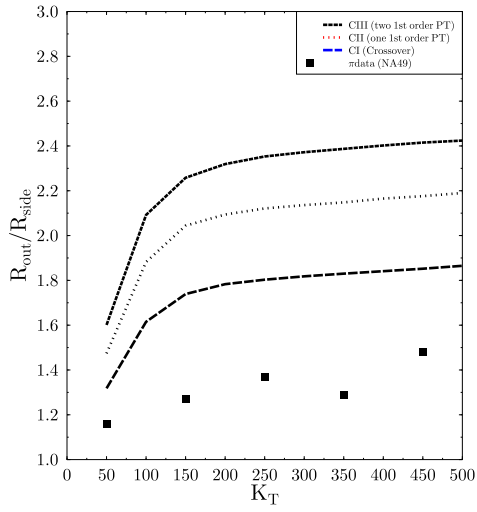


FIG .13. $R_{out}=R_{side}$ as a function of K_T at SPS for $T_f = 100M$ eV (left) and $T_f = 130M$ eV (right).

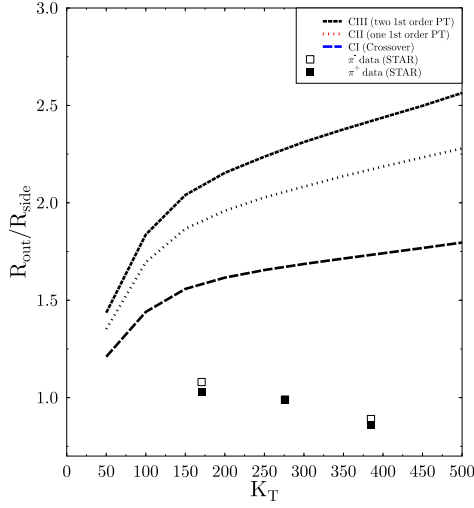


FIG .14. $R_{out}=R_{side}$ as a function of K_T at RHIC for $T_f = 80$ MeV .

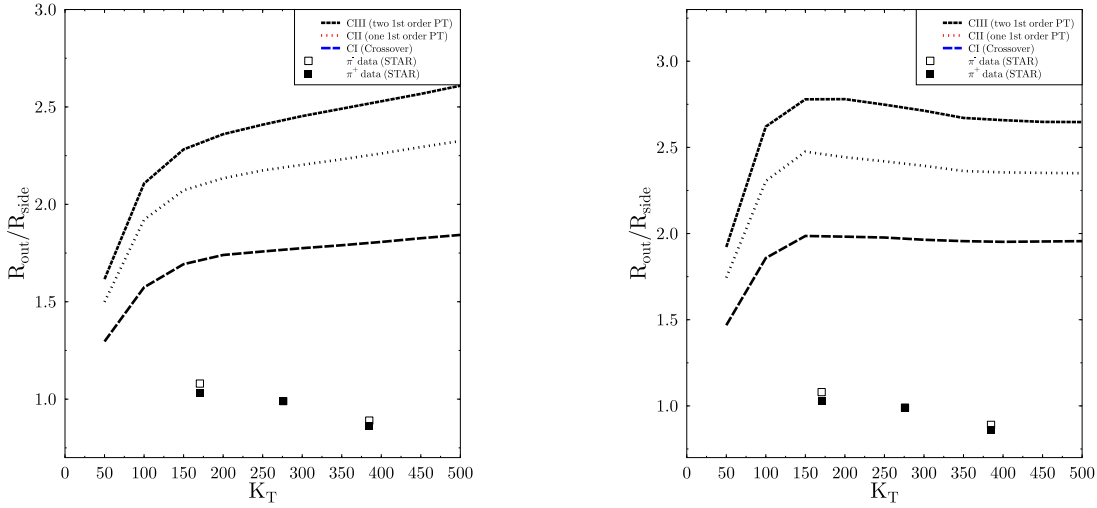


FIG .15. $R_{out}=R_{side}$ as a function of K_T at RHIC for $T_f = 100$ MeV (left) and $T_f = 130$ MeV (right).

One observes that at both energies the shortest lifetime of the system emerges from the EoS featuring a crossover (CI), while the slowest expansion results from the EoS with largest latent heat (CIII). At SPS energy, the data [34] yield a slowly rising $R_{out}=R_{side}$ ratio. This is obtained for all three EoS, if the freeze-out temperature is low, $T_f = 80; 100$ MeV. Of course, the absolute value of R_{out} is too large, while R_{side} is too small, the ratio comes out

way too large. As is obvious from the figures, we are not able to reproduce the data for $R_{\text{out}}=R_{\text{side}}$, though a small or even vanishing latent heat improves the picture. The best description is obtained for $T_f = 80 \text{ M eV}$.

Turning to RHIC, we see that the predicted general behavior of $R_{\text{out}}=R_{\text{side}}$ is similar as at the SPS, except a slight increase. That is because the larger initial entropy per baryon, which is deduced from the larger \sqrt{s} and p/p ratios, increases the lifetime of the system slightly. On the other hand, the preliminary STAR data [38] show $R_{\text{out}}=R_{\text{side}} > 1$, and a decrease with K_T . This behavior can evidently not be reproduced for low T_f . Larger freeze-out temperatures, $T_f = 130 \text{ M eV}$, lead to flat, or even slightly decreasing $R_{\text{out}}=R_{\text{side}}$. Nevertheless, $R_{\text{out}}=R_{\text{side}}$ is about a factor of 2 higher for $K_T = 100 \text{ M eV}$ as compared to the preliminary STAR-data.

IV . C O N C L U S I O N

The space-time evolution of ultra-relativistic heavy ion collisions at SPS and RHIC energies has been studied within hydrodynamic simulations using various EoS obtained from a chiral SU(3) SU(3) model. HBT-radii have been predicted for comparison to NA49- and STAR-data. The influence of different orders of the chiral phase transition and the underlying EoS have been accessed.

A small latent heat, i.e. a weak first-order chiral phase transition or even a smooth crossover, leads to higher r_T and smaller λ -values as well as to high R_{side} and smaller R_{out} HBT-values and are closest to the data in almost all cases. However, a quantitative description of the data, both at SPS energy as well as at RHIC energy, is not reached within the present hydrodynamical approach using the various SU(3) chiral EoS.

Apparently, conclusions can only be drawn after considerable improvements on various aspects of the description of high-energy heavy-ion collisions.

In particular, the effective chiral-SU(3) potential is rather rapidly varying around T_c . Therefore, a non-equilibrium description, accounting for supercooling effects and/or rapid

spinodal decomposition, might be in order [24,27]. In fact, it has been argued that the decay of a droplet of chirally symmetric matter from a region of negative pressure may yield smaller values for the HBT radii, as well as a smaller ratio $R_{out}=R_{side}$ [39]². Such considerations are out of the scope of the present manuscript but will be studied in detail in the future work. More realistic freeze-out descriptions [20,44] may improve the results. However, as dissipative effects are expected to prolong the lifetime of the pion source even more, it appears very likely that a quasi-adiabatic first-order phase transition with large latent heat, for which a hydrodynamical description should be adequate, can not describe the pion HBT data from CERN-SPS and from BNL-RHIC. This observation may be viewed as an experimental confirmation of the predictions from lattice QCD [2,21].

The nature of the chiral symmetry restoration will be better understood by analyzing forthcoming experimental data from RHIC. For example, correlations among kaons, protons, and non-identical particles can be analysed [40]. Excitation functions between CERN-SPS energy ($\sqrt{s} = 17.4$ A GeV) and the present BNL-RHIC energy ($\sqrt{s} = 130 - 200$ A GeV) would be extremely useful and might provide a more detailed view. The excitation functions of source sizes and lifetimes and also so-called "azimuthally sensitive" HBT-analysis [41] could be useful to obtain a complete picture of the phase transition via the structure of the pion source in space-time. With these data emerging, we hope that it will be possible to obtain a deeper understanding of the QCD phase transition in high-energy heavy-ion collisions.

A C K N O W L E D G E M E N T

We would like to thank A. Dumitru and D. Rischke for numerous discussions and for providing the relativistic hydrodynamics and the appropriate correlation function Codes. We also thank K. Bugaev, I. Mishustin and L. Satarov for discussions. This work was supported

²Note, however, that within our effective theory for chiral symmetry restoration the spinodal instability occurs before negative pressure is reached, see Fig. 3.

by Deutsche Forschungsgemeinschaft (DFG), Gesellschaft für Schwerionenforschung (GSI),
Bundesministerium für Bildung und Forschung (BMBF) and Graduiertenkolleg Theoretische
und experimentelle Schwerionenphysik.

REFERENCES

- [1] R. D. Pisarski and F. Wilczek, *Phys. Rev. D* 29, 338 (1984).
- [2] F. R. Brown et al., *Phys. Rev. Lett.* 65, 2491 (1990); Y. Iwasaki, K. Kanaya, S. Kaya, S. Sakai and T. Yoshie, *Z. Phys. C* 71, 343 (1996).
- [3] G. Goldhaber, S. Goldhaber, W. Lee and A. Pais, *Phys. Rev.* 120, 300 (1960).
- [4] E. Shuryak, *Phys. Lett. B* 44, 387 (1973); M. Gyulassy, S. K. Kaumann and L. W. Wilson, *Phys. Rev. C* 20, 2267 (1979); A. Makhlin and Y. Sinyukov, *Z. Phys. C* 39, 69 (1988); Y. Hamada and S. S. Padula, *Phys. Rev. D* 37, 3237 (1988).
- [5] K. Kajantie and L. McLerran, *Ann. Rev. Nucl. Part. Sci.* 37, 293 (1987); J. W. Harris and B. Muller, *Ann. Rev. Nucl. Part. Sci.* 46, 71 (1996); S. A. Bass, M. Gyulassy, H. Stocker and W. Greiner, *J. Phys. G* 25, R1 (1999).
- [6] R. M. Weiner, *Phys. Rept.* 327, 249 (2000); T. Csorgo, hep-ph/0001233.
- [7] U. Wiedemann and U. Heinz, *Phys. Rept.* 319, 145 (1999).
- [8] S. Pratt, *Phys. Rev. D* 33, 1314 (1986); G. Bertsch, M. Gong, M. Tohyama, *Phys. Rev. C* 37, 1896 (1988); G. Bertsch, *Nucl. Phys. A* 498, 173c (1989).
- [9] B. R. Schlei, U. Omik, M. Plumer and R. M. Weiner, *Phys. Lett. B* 293, 275 (1992); J. Bolz, U. Omik, M. Plumer, B. R. Schlei and R. M. Weiner, *Phys. Rev. D* 47, 3860 (1993); *Phys. Lett. B* 300, 404 (1993).
- [10] D. H. Rischke and M. Gyulassy, *Nucl. Phys. A* 608, 479 (1996)
- [11] L. D. Landau and E. M. Lifshitz, "Fluid Mechanics", Pergamon Press, New York, 1959
- [12] K. Kajantie and L. McLerran, *Phys. Lett. B* 119, 203 (1982); *Nucl. Phys. B* 214, 261 (1983); J. D. Bjorken, *Phys. Rev. D* 27, 140 (1983); G. Baym, B. L. Friman, J. P. Blaizot, M. Soyeur, and W. Czyz, *Nucl. Phys. A* 407, 541 (1983); K. Kajantie, R. Raitio, and P. V. Ruuskanen, *Nucl. Phys. B* 222, 152 (1983)

- [13] e.g. H. Stocker et al., *Phys. Rev. C* 25, 1873 (1982); *Nucl. Phys. A* 566, 15C (1994); R. Venugopalan, M. Prakash, M. Kataja and P. V. Ruuskanen, *Nucl. Phys. A* 566, 473C (1994); A. Dumitru, et al., *Phys. Rev. C* 51, 2166 (1995); B. R. Schlei, U. O. Mik, M. Plumer, D. Strottman and R. M. Weiner, *Phys. Lett. B* 376, 212 (1996); J. Brachmann et al., *Phys. Rev. C* 61, 024909 (2000); K. Morita, S. Muroya, H. Nakamura and C. Nonaka, *Phys. Rev. C* 61, 034904 (2000).
- [14] A. Dumitru and D. H. Rischke, *Phys. Rev. C* 59, 354 (1999).
- [15] D. H. Rischke, S. Bernard, and J. A. Manuh, *Nucl. Phys. A* 595, 346 (1995)
- [16] D. H. Rischke and M. Gyulassy, *Nucl. Phys. A* 597, 701 (1996)
- [17] P. Papazoglou, D. Zschesche, S. Schramm, J. Schaner-Bielich, H. Stocker, and W. Greiner, *Phys. Rev. C* 59, 411 (1999).
- [18] D. Zschesche, P. Papazoglou, S. Schramm, C. Beckmann, J. Schaner-Bielich, H. Stocker, and W. Greiner, *Springer Tracts in Modern Physics* 163, 129 (2000).
- [19] H. A. Weldon, *Z. Phys. C* 54, 431 (1992); M. Prakash, M. Prakash, R. Venugopalan and G. Welke, *Phys. Rept.* 227, 321 (1993); K. Haglin and S. Pratt, *Phys. Lett. B* 328, 255 (1994).
- [20] S. So, S. A. Bass and A. Dumitru, *Phys. Rev. Lett.* 86, 3981 (2001); S. A. Bass, A. Dumitru, M. Bleicher, L. Bravina, E. Zabrodin, H. Stocker and W. Greiner, *Phys. Rev. C* 60, 021902 (1999).
- [21] E. Laermann, *Nucl. Phys. A* 610, 1c (1996)
- [22] B. D. Serot and J. D. Walecka, *Int. J. Mod. Phys. E* 6, 515 (1997)
- [23] J. Theis, G. Graebner, G. Buchwald, J. A. Manuh, W. Greiner, H. Stocker and J. Polonyi, *Phys. Rev. D* 28 (1983) 2286.
- [24] A. Chodos, F. Cooper, W. Mao and A. Singh, *Phys. Rev. D* 63, 096010 (2001); O. Scav-

- enius, A. Dumitru, E. S. Fraga, J. T. Lenaghan and A. D. Jackson, Phys. Rev. D 63, 116003 (2001).
- [25] C. Greiner, P. Koch and H. Stocker, In Heavy Ion Collisions," Phys. Rev. Lett. 58 (1987) 1825; C. Greiner, D. Rischke, H. Stocker and P. Koch, Phys. Rev. D 38 (1988) 2797; C. Greiner and H. Stocker, Phys. Rev. D 44 (1991) 3517; C. Spieles, H. Stocker and C. Greiner, Eur. Phys. J. C 2 (1998) 351 [nucl-th/9704008].
- [26] D. Ardouin et al., Phys. Lett. B 446 (1999) 191.
- [27] A. Dumitru and R. D. Pisarski, hep-ph/0010083; O. Scavenius, A. Dumitru and A. D. Jackson, hep-ph/0103219.
- [28] A. Chodos, R. L. Jaffe, K. Johnson, C. B. Thorn, and V. F. Weisskopf, Phys. Rev. D 9, 3471 (1974)
- [29] J. Letessier, A. Tounsi, U. Heinz, J. Sollfrank and J. Rafelski, Phys. Rev. Lett. 70, 3530 (1993); P. Braun-Munzinger, I. Heppke and J. Stachel, Phys. Lett. B 465, 15 (1999); D. Zschesche, P. Papazoglou, C. W. Beckmann, S. Schramm, J. Schauer-Bielich, H. Stocker and W. Greiner, Nucl. Phys. A 663, 737 (2000).
- [30] K. Geiger and J. I. Kapusta, Phys. Rev. D 47, 4905 (1993)
- [31] T. Schonfeld, H. Stocker, W. Greiner, and H. Sorge, Mod. Phys. Lett. A 8, 2631 (1993)
- [32] H. Stocker et al., in Proc. 4th Int. Workshop "Relativ. Aspects of Nucl. Phys.", Rio de Janeiro 1995 (Brazil) (eds. T. Kodama, K. C. Chung, Y. Hamada, G. Odyniec, H. Strobele, C.-Y. Wong), World Scientific, Singapore, 1996, p. 437
- [33] S. E. Vance, M. Gyulassy and X. N. Wang, Nucl. Phys. A 638 (1998) 395C [nucl-th/9802036].
- [34] C. B. Lum e, talk given at Quark Matter 2001, Jan. 15{20, Stony Brook, NY, USA .
- [35] A. Makhlin and Y. Sinyukov, Z. Phys. C 39, 69 (1988); Y. Hamada and S. S. Padula,

- Phys. Rev. D 37, 3237 (1988).
- [36] T. Csongó, B. Lorstad and J. Zimanyi, Z. Phys. C 71, 491 (1996).
- [37] S. Pratt, Phys. Rev. Lett. 53, 1219 (1984); Phys. Rev. C 49, 2722 (1994).
- [38] STAR collaboration: "Pion Interferometry of $\sqrt{s_{NN}} = 130$ GeV Au+Au collisions at RHIC", submitted to Phys. Rev. Lett
S. Y. Panitkin, nucl-ex/0106018.
- [39] T. Csongó and L. P. Csernai, Phys. Lett. B 333, 494 (1994).
- [40] S. Panitkin, talk given at Quark Matter 2001, Jan. 15-20, Stony Brook, NY, USA.
- [41] M. A. Lisa, U. Heinz and U. A. Wiedemann, Phys. Lett. B 489, 287 (2000); M. A. Lisa et al. [E895 Collaboration], Phys. Lett. B 496, 1 (2000); nucl-ex/0104012.
- [42] A. Muronga, nucl-th/0104064.
- [43] N. Xu and M. Kaneta, nucl-ex/0104021; P. Braun-Munzinger, D. Magestro, K. Redlich and J. Stachel, hep-ph/0105229.
- [44] K. A. Bugaev, Nucl. Phys. A 606, 559 (1996); V. K. Magas et al., Heavy Ion Phys. 9, 193 (1999); C. Anderlik et al., Phys. Rev. C 59, 3309 (1999).